



A Journal of



Accepted Article

Title: Chemical and electrochemical oxidations of tris(3,5-di-tert-butylphenyl)phosphine. High Z' crystal structures and conformational effects associated with bulky meta substituents

Authors: Ivelise Dimbarre Lao Guimarães, Jarem Raul Garcia, Karen Wonhrath, and René T. Boéré

This manuscript has been accepted after peer review and appears as an Accepted Article online prior to editing, proofing, and formal publication of the final Version of Record (VoR). This work is currently citable by using the Digital Object Identifier (DOI) given below. The VoR will be published online in Early View as soon as possible and may be different to this Accepted Article as a result of editing. Readers should obtain the VoR from the journal website shown below when it is published to ensure accuracy of information. The authors are responsible for the content of this Accepted Article.

To be cited as: *Eur. J. Inorg. Chem.* 10.1002/ejic.201800656

Link to VoR: <http://dx.doi.org/10.1002/ejic.201800656>

WILEY-VCH

Chemical and electrochemical oxidations of *tris*(3,5-di-*tert*-butylphenyl)phosphine. High *Z'* crystal structures and conformational effects associated with bulky *meta* substituents.Ivelise Dimbarre Lao Guimarães,¹ Jarem Raul Garcia,¹ Karen Wohnrath*¹ and René T. Boéré*^{2,3}¹ Departamento de Química, Universidade Estadual de Ponta Grossa 84030-900, Ponta Grossa, Paraná, Brazil² Department of Chemistry and Biochemistry, University of Lethbridge, Lethbridge, Alberta T1K 3M4, Canada³ Canadian Centre for Advanced Fluorine Technologies, University of Lethbridge, Lethbridge, Alberta T1K 3M4**Abstract**

Synthesis and single crystal X-ray diffraction structures of (3,5-^tBu₂-C₆H₃)₃P, (3,5-^tBu₂-C₆H₃)₃PO·H₂O, (3,5-^tBu₂-C₆H₃)₃PS and (3,5-^tBu₂-C₆H₃)₃PSe are reported. The structure of (3,5-^tBu₂-C₆H₃)₃P has *Z'* = 4, with both *M* and *P* enantiomers of a helical conformation and a conformation with one flat ring in the same lattice. The pyramidity index, $\sum\{\angle\text{CPC}\}$, is smaller for the helical compared to the flat conformers. All four have structures that are more pyramidal than the corresponding Ph₃P(E) derivatives, which is attributed to stronger intramolecular dispersion forces. The oxide crystallizes with *Z'* = 2 as a water-bridged dimer that is the most separated such dimer amongst 26 known structures, providing evidence for a distal (or perimeter) steric effect. Cyclic voltammetry in CH₃CN/[ⁿBu₄N][ClO₄] indicated anodic peak potentials of +0.785 V for (3,5-^tBu₂-C₆H₃)₃P, +0.745 for (3,5-Me₂-C₆H₃)₃P, +0.735 V for (4-MeO-3,5-Me₂-C₆H₃)₃P and +0.535 V for (4-MeO-C₆H₃)₃P, all relative to Fc⁺⁰. On this scale, Ph₃P oxidizes at +1.04 V. The unexpectedly high oxidation potentials for the first three phosphines is attributed to a more pyramidal structure resulting in lowering of the HOMO energy compared to expectations from Hammett constants and ¹J(P,Se) NMR coupling constants.

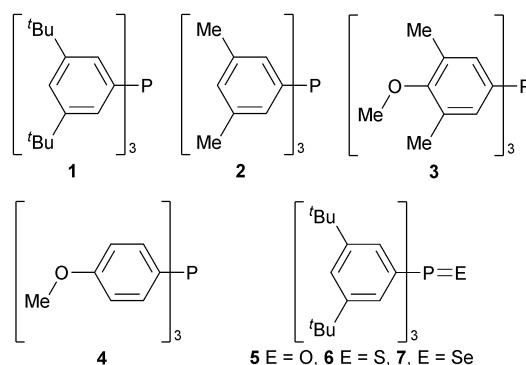
Keywords:

triarylphosphane; donor strengths from voltammetry; racemization of propeller molecules; London dispersion forces; empirical dispersion corrections

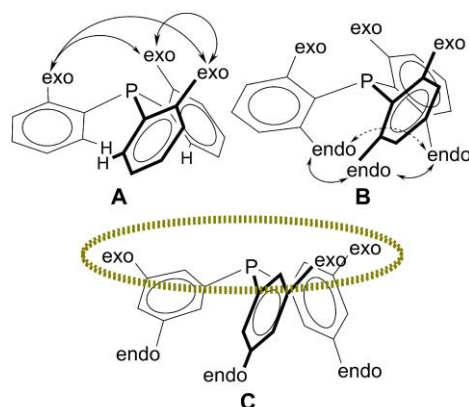
Introduction

Phosphines remain amongst the most important ligands in transition metal coordination and organometallic chemistry with applications to catalysis,¹⁻⁴ are very important Lewis bases for frustrated Lewis pair (FLP) chemistry⁵ and are used in critically important organic processes such as the Mitsunobu reaction.⁶ Triarylphosphines are still the most diverse and commonly employed phosphines. Molecules in the class Ar_3P and $\text{Ar}_3\text{P}=\text{E}$ ($\text{E} = \text{O}, \text{S}, \text{Se}$) have long been important to the isomerization and energetics of propeller-shaped molecules based on foundational work of Mislow on triarylmethanes.⁷⁻⁹ His group established the strong connection of experiment (originally from dynamic NMR spectroscopy) with pioneering work in computational stereochemistry.¹⁰ Interest in this area remains strong amongst triarylphosphines,¹¹⁻¹⁴ triarylphosphine chalcogenides,^{15,16} and conformations of Ar_3P ligands in coordination complexes.¹⁷⁻²¹

We are exploring a series of substituted triarylphosphines **1** - **4** with different donor strengths and hydrophobicity.²² Whereas **2** - **4** are commercially available,²³⁻²⁵ the title phosphine *tris*(3,5-di-*tert*-butylphenyl)phosphine, **1**, was, at the time our study commenced, only reported in a single communication and remained incompletely characterized.⁴ In particular, the crystal structure has not been reported.



Our extensive experience with hydrophobic phosphines bearing bulky 2,6-substituents, such as *tris*(2,6-diisopropylphenyl)phosphine (Dipp_3P),^{26,27} *tris*(2,4,6-triisopropylphenyl)phosphine (Tripp_3P)²⁸ and *tris*(2,4,6-trimethylphenyl)phosphine (Mes_3P),²⁹ was not transferable to our target ruthenium complexes as they are too sterically congested to coordinate to the metal and we thus turned to analogous 3,5-disubstituted ligands. We were particularly attracted to **1** and **2** but for completeness included 4-MeO substituted phosphine **3** and the corresponding **4** (which is one of the most basic Ar_3P). Solution redox potentials have been recognized as excellent measures of phosphine donor ability and thus the voltammetric behaviour of the series **1** - **4** have been determined.^{26,27,30-32} Since chalcogenides of **1** were not known and no crystal structures of the series **1**, **5** - **7** has been reported, we synthesized them all and determined their structures to obtain pyramidity indices (i.e. the sum of the angles around phosphorus, $\sum\{\angle\text{CPC}\}$)³³ for comparison to bulky 2,6-disubstituted phosphines.²⁶⁻²⁹ It is now recognized that different types of steric effects can occur in pyramidal phosphines. Systematic substitution in the 2-position provides *steric shielding* (Scheme 1A) by creating a cavity around the Lewis-basic electron density of the highest occupied molecular orbital (HOMO). This occurs when all the substituents are oriented *exo*, as is commonly but not exclusively observed in coordination complexes.³³ However, systematic 2,6-disubstitution also generates *steric pressure* (Scheme 1B) between the *endo* substituents. This repulsive interaction can significantly decrease the pyramidity of PAR_3 , which raises the HOMO energy (inducing greater basicity) and enhances the steric shield by forcing the *exo* substituents closer around the phosphorus donor.^{26,33} Systematic 3-substitution provides an opportunity for the flanking *exo* groups to create a coordination pocket (dashed perimeter in Scheme 1C) without direct interference with the donor site (distal steric bulk).³⁴⁻³⁷ But does 3,5-disubstitution also generate steric pressure from the *endo* substituents? The title compound **1** and its chalcogenides **5** - **7** can help answer this question.



Scheme 1. Steric effects in substituted PAR_3

The crystal structures of **1** and **5** – **7** proved to be challenging due to a variety of disorder phenomena, especially **1** which crystallizes from numerous solvents, as well as by sublimation, in an unusual lattice with four molecules in the asymmetric unit ($Z' = 4$). There is a growing awareness of crystal structures with values of $Z' > 1$,^{38,39} the incidence of which has steadily been rising and achieved 16% of all organic structures compiled in the Cambridge Crystallographic Database (CSD)⁴⁰ in 2016. It is likely that this increasing incidence reflects improvements in crystallographic technology (hardware and software) since structures with more than one equivalent chemical entity in the asymmetric unit are usually more difficult to solve and to refine to publication quality. Nevertheless, higher values still remain extremely rare so that the incidence of $Z' > 2$ is only 1.23% in the CSD (2016).

During the course of our work, several new papers were published which independently reported the synthesis and utilization of **1**,^{2,3,6} thus generating significant interest in a phosphine that has lain dormant for some twenty years. The main purpose of this paper is to provide evidence for the relative donor strengths for **1** – **4** and to explore steric effects from 3,5-disubstitution in the structures of **1** and its derivatives.

Results and Discussion

Synthesis. We prepared **1** by modifying the original report of Manabe to facilitate workup under anaerobic conditions, using canula techniques.⁴ Although the reactions are essentially quantitative (confirmed by NMR and mass balance), purification proved difficult and all the reported preps suffer in recovered yield.^{2,3,6} This seems to be due to the extremely high solubility of **1** in alcohols. Crystallographic investigation demonstrated that growing crystals free of oxide contamination was especially difficult (see SI for details). The oxide **5** was therefore made deliberately to confirm this contaminant spectroscopically (see below). We eventually found that recrystallization from a minimum quantity of cold 3:1 MeOH/EtOH under N_2 affords small colourless needles of pure **1**.

Crystal structure of 1. Single crystal X-ray diffraction provides the structure of **1** which has the same habit (small colourless long thin plates) and unit cells when grown from ethanol or methanol as recrystallization solvents and also when grown by sublimation in a gradient furnace. The structure is complicated, with 4 independent molecules in the $\text{P2}_1/\text{c}$ lattice (denoted as $Z' = 4$, see Table S1 in the SI). These exist as two distinct conformational isomers; the one shown in Figure 1a has aryl ring C1 > C6 oriented 'flat', i.e. orthogonal to a plane that contains the principal axis of the whole molecule through P1 and the non-bonded electrons on phosphorus. The other three have the common helical arrangement of all three rings (Figure 1b), with approximate three-fold rotational symmetry. The two types of conformations are depicted in perspective in Figure 1c in idealized form to facilitate discussion. Additionally, within the asymmetric unit (as denoted by the phosphorus atoms), P100 has an anti-clockwise rotation (P configuration – see Figure S13 in the Supporting Information – SI)^{13,18,41} if viewed from above while P200,300 have clockwise rotation (M).⁴²

Three of the four molecules have significant rotational positional disorder of the ^tBu rings that could be modelled with part occupancies (see the SI). The independent molecules also show a distribution of limiting conformations of the ^tBu groups w.r.t. the attached aryl planes; in the four rotationally disordered groups, the components are close to these two limiting conformations. The observed (Fig. 1c) limiting conformations of the ^tBu groups have one in-plane methyl group either *syn* with the side of the phenyl ring (red colour) or *anti* (green colour).

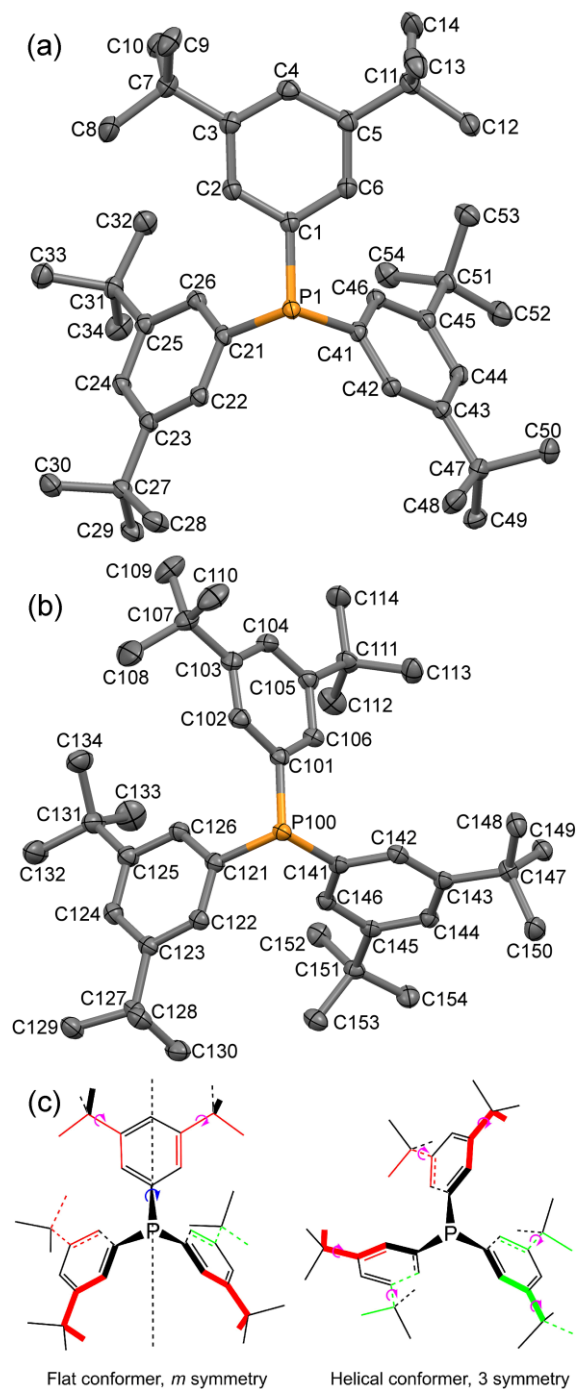


Figure 1. Displacement ellipsoids plots (30% probability) of (a) the 'flat' conformation designated by P1 containing C1→54 and (b) one of the helical conformations designated by P100. Only the major components of the two-part rotational disorder model for ^tBu groups C11 and C47 are shown. Hydrogen atoms are omitted and the atom numbering scheme of x1–x14 for the 12 aryl rings is provided. (c) Perspective diagrams of the P1 and P300 molecules for the major ^tBu conformations in the crystal structure.

High Z' in Ar_3P and Ar_3PE . The Durham High Z' database for $Z' > 4$ ⁴³ has no entries for Ar_3P and Ar_3PE ($\text{E} = \text{O}, \text{S}, \text{Se}$). A review of the CSD entries (CSD Version 5.39, November 2017) reported 108 Ar_3P structures with $Z' = 2$ and 72 for Ar_3PO . For $Z' = 3$, there were two entries for Ar_3P and four for Ar_3PO , while for $Z' = 4$, there were just 11 Ar_3P and 5 Ar_3PO examples. Thus, the incidence of $Z' > 1$ for triarylphosphines is low both in number and range. Intriguingly, one of two polymorphs of *tris*(3,5-*bis*(trifluoromethyl)phenyl)phosphine (CSD refcode: IGAGIG), a close structural analogue to **1** in view of the similar molecular size of CF_3 and ^tBu substituents, also crystalizes with $Z' = 4$.^[44] Moreover, in that structure three of the four molecules are predominantly in a 'flat' conformation and only one is helical. Furthermore, unlike **5** – **7**, the oxide and selenide of this fluorinated phosphine all adopt the flat conformation in their respective crystal structures.^{45,46}

Computational analysis of conformation. It was thus important to ascertain which of the two, 'flat' or helical, is the lower energy in **1** and what the energy difference between conformers is. Hybrid DFT calculations were undertaken at the B3LYP/6-31G(2d,p) level of theory and an optimization that starts with the flat conformer as found in the crystal structure (Figure 1a) smoothly converts over to a helical geometry. The most optimized flat geometry was found to be about $6 \text{ kJ}\cdot\text{mol}^{-1}$ higher in energy than the optimized helical conformation.

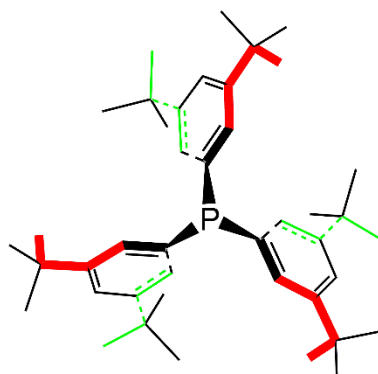


Figure 2. DFT minimum-energy conformer: symmetry point group 3, with the upper ^tBu groups oriented with a co-planar methyl group *syn* (red) and all the lower ^tBu groups oriented *anti* (green colour).

Once it was found that the helical form is the most stable, attention was paid to the limiting conformations of the ^tBu groups. Whereas in the geometry taken from the X-ray structure, five ^tBu groups are oriented with one methyl group in-plane with the attached aryl rings and in *syn* conformation and the sixth is found *anti*, the 3-fold symmetric conformation wherein all three *exo* ^tBu groups (i.e. on the phosphorus atom side of the pyramid) are *syn* and the three *endo* groups all *anti* (Figure 2) is the lowest-energy at this level of theory. By contrast, alternatives with one of the lower groups *anti* and the other two *syn* is $\sim 1.5 \text{ kJ}\cdot\text{mol}^{-1}$ higher and the more symmetric analogue with *all* the lower groups *syn* is $\sim 2.3 \text{ kJ}\cdot\text{mol}^{-1}$ higher in energy than that of the calculated lowest energy conformer. Such small energy differences are certainly consistent with the presence of rotationally disordered ^tBu groups in the reported crystal structure (see above). For the same reason it is evident that thermal energy at RT is also capable of promoting the P1 molecule found in the crystal structure of **1** to a flat conformation ($\sim 6 \text{ kJ}\cdot\text{mol}^{-1}$).

This geometry with optimal ^tBu group orientations (Fig. 2) was then used in a 'relaxed scan' algorithm by stepping one fixed C-P-C-C dihedral angle (C1-P1-C21-C26) with variable step sizes to investigate any influence of the bulky 3,5-substituents on the phosphine racemization mechanism (Figure 3). This follows the classical algorithm of Mislow for computational investigation of conformation.⁸ For comparison, a similar relaxed scan at the same level of theory was undertaken for the 'parent' phosphine PPh_3 . The scans were undertaken over approximately 180° . For PPh_3 starting from the *M* helical enantiomer, **i**, the energy rises to a maximum **ii** at about $5.6 \text{ kJ}\cdot\text{mol}^{-1}$, with a 'flat' orientation of one ring, in accordance with the determination

by Mislow that the two-ring flip is the threshold mechanism for racemization of triaryl pyramidal molecules (Figure S13).^{7,8,13} Beyond this maximum, the *P* helical structure **iii** is achieved. Further driving of the dihedrals leads to a second 'flat' conformation **iv** at 5.1 kJ·mol⁻¹, that differs slightly from **ii** in the relative twists of the other two phenyl rings and then rapidly falls off to a final helical *M* geometry **v** that is identical to **i**. None of this is surprising, but when the same scan is undertaken on the optimized geometry of **1**, starting from the *M* ground state **I**, the energy rises steeply and reaches a different maximum **II** at about 26 kJ·mol⁻¹, for which the geometry is very close to the idealized intermediate of Mislow's one-ring flip mechanism (one aryl ring parallel to the principal axis). At **III** the *P* enantiomer is attained (which can be further optimized to the same energy as **I**). Further driving of the dihedral leads to **IV** at 6.7 kJ·mol⁻¹, with the single 'flat' aryl ring. Fascinatingly, the energy barrier for the intermediates **IV** and **iv** are extremely similar despite the large differences in substituent bulk. Thus, **1** can be expected to shuttle back-and-forth over the barrier at **IV** to interconvert its chirality (and **III**, **IV** and **V** co-exist in the lattice of the *Z'* = 4 crystal structure – as discussed above).

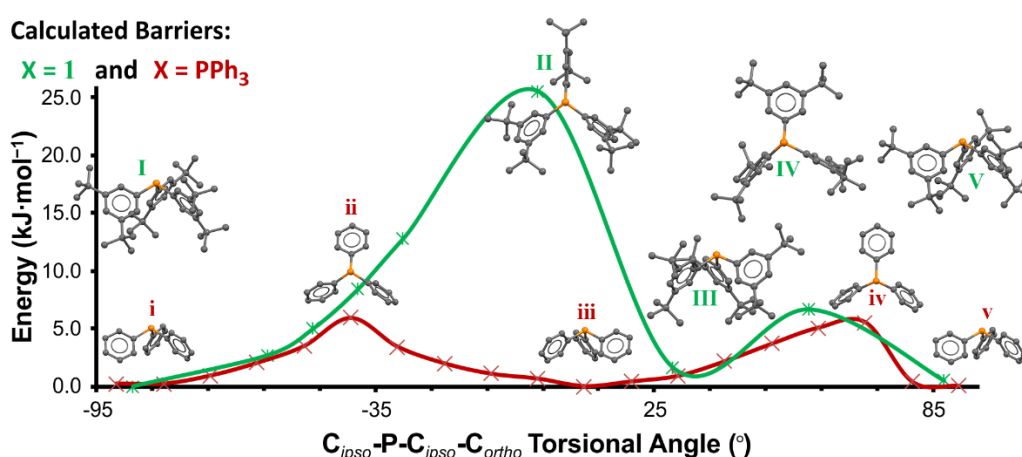


Figure 3. Comparative computed energy scans at the B3LYP/6-31G(2d,p) level of theory for **1** (green) and PPh₃ (red) with full optimization of all parameters other than the $C_{ipso}\text{-P-C}_{ipso}\text{-C}_{ortho}$ torsion angles. Molecular conformations for the energy maxima and minima are also depicted (see text for further details).

Electrochemical oxidations and phosphine donor strengths. The electrochemical properties of phosphines **1–4** and PPh₃ were studied by cyclic voltammetry (CV) in CH₃CN/[ⁿBu₄N][ClO₄] solutions and representative voltammograms are presented in Figure 4a. The CVs show the presence of an irreversible oxidation process with anodic peak potentials (E_p^a) in the range +0.54 to +0.79 V. Scan-rate dependencies correlated linearly with the square root, indicating diffusion-controlled processes (see Figure S11). Irreversible oxidations for phosphines lacking enhanced steric shielding (Scheme 1B) is normal and has been attributed to rapid reaction with adventitious water.²⁷ Despite this, good correlations of the anodic peak potentials have been obtained to the relative basicity of phosphines.^{30–32} The range of potentials in **1–4**, 0.25 V, is reasonably large for this variation in substituents. Phosphines **2**, **4** and PPh₃ were measured previously in a comparative investigation, albeit under very different conditions (data included in Table 1).⁴⁷ These results agree well in the relative placement of **2** between **4** and PPh₃ (potential steps of 0.17 V and 0.18 V, compared to ours of 0.29 V and 0.21 V). Geometry optimized B3LYP/6-31G(2d,p) DFT calculations, incorporating Grimme's D3 empirical dispersion correction, were performed on **1–4**, and the energy of the HOMO of each phosphine is also listed in Table 1. Electrochemical oxidation involves the removal of an electron from this orbital (Figure 4c, inset). The oxidation potential data correlates linearly with the HOMO energies, yielding an R^2 of 0.97 (Figure 4b). By contrast, the Hammett σ^+ constants make the wrong prediction, especially for **3** (see Figure S12).

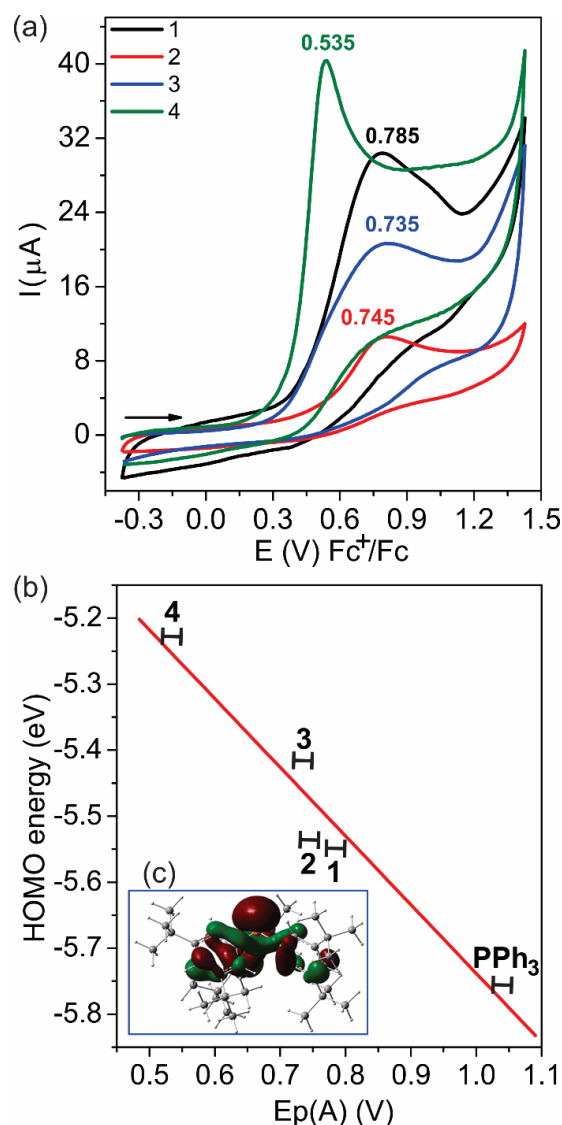


Figure 4. (a) Cyclic voltammograms of phosphines **1** - **4** in $\text{CH}_3\text{CN}/[\text{nBu}_4\text{N}][\text{ClO}_4]$ solutions measured vs. Ag/AgCl and expressed on $\text{Fc}^{+/0}$ scale. (b) Relative basicity of **1** - **4** and PPh_3 from the correlation between E_p^a and DFT HOMO energies ($R^2 = 0.97$). (c, inset) Kohn-Sham orbital surface diagram for the redox molecular orbital of **1**.

Table 1. Experimental voltammetric data and DFT computed redox orbital energies

Phosphine	E_p^a , V ^a	ΔE to 1 , V	Culcasi, V ^b	HOMO, eV	Hammett σ^+ ^c	$\sum\{\angle\text{CPC}\}$, ^{od}
PPh_3	+1.04 ^e	-0.251	+1.40	-5.755	0	305.1
1 (3,5- ^t Bu ₂ -C ₆ H ₄) ₃ P	+0.785	0.000		-5.549	-0.118	298.3
2 (3,5-Me ₂ -C ₆ H ₄) ₃ P	+0.745	0.025	+1.22	-5.536	-0.132	304.8
3 (4-MeO-3,5-Me ₂ -C ₆ H ₄) ₃ P	+0.735	0.039		-5.416	-0.91	304.8
4 (4-MeO-C ₆ H ₄) ₃ P	+0.535	0.251	+1.05	-5.228	-0.778	305.4

^a Measured in $\text{CH}_3\text{CN}/[\text{nBu}_4\text{N}][\text{ClO}_4]$ solutions vs. Ag/AgCl and scaled to $\text{Fc}^{+/0}$ at the invariant internal $E_{1/2} = +0.375$ V. Estimated error = ± 0.010 V ^b Determined by CV in *n*-butyronitrile vs. SCE.⁴⁷ ^c From ref. 48. ^d From geometry-optimized B3LYP/6-31G(2d,p) hybrid DFT calculations incorporating Grimme's D3 empirical dispersion corrections. ^e From ref. 26.

According to both the voltammetric data from our study and that of Culcasi *et al.*, as well as the calculated HOMO energies, **1** – **3** cluster together with similar donor strengths roughly half-way along the range between PPh₃ and very basic **4**. A different way to establish phosphine donor ability is the well-known correlation between one-bond ⁷⁷Se-³¹P NMR coupling constant and pK_b.⁴⁹ Since we have prepared the selenide **7** in bulk (see below), it was possible to accurately measure its coupling constant as ¹J(⁷⁷Se, ³¹P) = 719 Hz. Using the empirical correlation of Beckmann *et al.* and restricting to just Ar₃P entries rather than all triorganophosphines, this provides an estimate of pK(b) ≈ 10.2, which places **1** close to (4-CH₃C₆H₄)₃P in basicity.⁴⁹ There is thus a significant discrepancy between the donor ability established from the direct Se-P coupling constant and the voltammetry.

Chemical oxidations. In addition to voltammetry, chemical oxidations of **1** were undertaken with oxygen, sulfur and selenium. Full characterization details are provided in the Experimental section and the crystal structures were determined. While this work was in progress, brief reports have appeared independently for the preparation of oxide **5**² and selenide **7**³ with partial characterization for each.

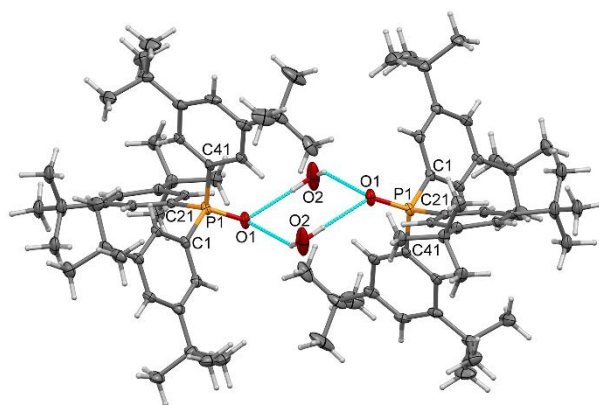


Figure 5. Displacement ellipsoids plot (40% probability) of one of the two crystallographically independent and centrosymmetric water-bridged dimers of **5** as found in the crystal lattice. H atoms not involved in H-bonding and minor components of disordered ^tBu groups have been omitted for clarity. The water O2 atoms are centered on a plane also containing the two P1 atoms of the asymmetric unit.

The oxide crystallizes as two independent centrosymmetric water-bridged dimers ($Z' = 2$; Figure 5). However, the presence of a superlattice provides an alternative refinement with $Z' = 4$ (see Figure S3); on comparison of the two models, no significant advantage obtains from the superlattice as both models involve disorder. One of the two dimers is depicted in Figure 5 involving water atoms O2 and the P1-O1 atoms. Notably, the second dimer involving water atoms O3 and the P100-O100 atoms was found to have only 0.65 occupancy for the water and is also a less compact dimer. The O \cdots OH₂ contact distances in the depicted dimer are 2.861(2) and 2.981(3) Å, averaging to 2.921 Å, whereas for the P100 structure the distances are 2.902(6) and 3.065(6) Å. A search of the CSD (Nov 2016) found 25 structures in which two phosphine oxide units are bridged by two water molecules in a manner analogous to **5** (see Table S3). The full range of individual contacts in this search is from 2.649 – 2.930 Å, but the *average* within a given structure ranges from 2.680 – 2.901 Å. By both criteria, the dimers in **5** have the longest O1 \cdots O1' distances of the set. This suggests that the steric repulsion in **5** between *meta* ^tBu substituents on adjacent molecules of the bridged dimer is significant (for a space-filling representation of the dimers see Figure S4). In other words, this suggests the existence of distal steric effects also in **5** (see above, Scheme 1c).

The torsion angles O–P–C_{2,22,42} and O–P–C_{102,122,142} are all different: 26.7(2), 25.0(2), 35.7(7) and 31.3(2), 13.9(2), 54.3(2) so that the geometry of the P100/O100 molecule approximates to the Mislow one-ring flip intermediate (one aryl ring co-planar with the principal axis – see Figure S13).^{7,8,13} By contrast the

P1/O1 molecule is closer to helical. The average P=O distance in **5** is 1.4925(10) Å, which is identical to the average 1.494(6) Å for the 25 comparative water bridged dimers in Table S3 and perhaps slightly longer than a global average for 700 Ar₃P=O found in the CSD of 1.488(13) Å.

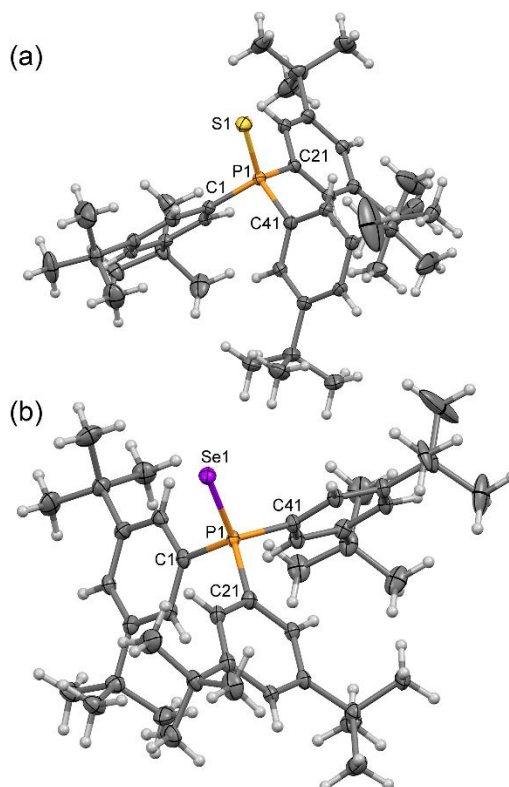


Figure 6. Displacement ellipsoids plots (40% probability) depicting the molecular structure of (a) **6** and (b) **7** as found in their crystal lattices. Minor components of disordered ^tBu groups, as well as Se and P in **7**, are omitted (see the ESI).

The crystal structures of sulfide **6** and selenide **7** are isostructural in $P2_1/c$ (Figure 6). The data for **7** were determined several times but always display some strange ghosting of heavy atom sites, leading to large residual peaks in the refinement. No suitable twin law could be found to deal with this issue but the refinement as a whole-molecule disorder is otherwise unexceptional. The two structures display ^tBu disorders for the same groups, likely reflecting regions of lesser interactions in the lattice. Both lattices also contain voids (67 Å³, 1.7% of cell volume for **6**; 141 Å³, 3.5% of cell volume for **7**) but the volumes of these voids are too small to be solvent accessible. There are no significant intermolecular contacts in either structure.

The torsion angles S–P–C–C_{2,22,42} are 50.2(2), 40.7(2), 42.4(2) in **6** and Se–P–C–C_{2,22,42} are 49.7(3), 39.0(3), 44.5(3) in **7**. Thus, these essentially isostructural molecules are both closer to an ideal helical geometry with three-fold rotational symmetry than are either of the independent oxides. The P–S bond distance in **6** is 1.9596(8), which is well within the mean of 1.953(11) Å for 179 Ar₃PS reported in the CSD. The P–Se distance in **7** is 2.115(1), also entirely normal compared to the mean 2.115(14) Å for 84 Ar₃PSe in the CSD.

Phosphine pyramidality. We recently defined a pyramidal index, $\sum\{\angle\text{CPC}\}$, to help define the shapes of organophosphines and related molecules using internal geometries from crystal structures or computation.^{33,50} An index of 360° is trigonal planar and 280.8° is the almost right-angled geometry achieved in PH₃. Compared to the latter, three aryl rings cause significant reduction in pyramidal

$\Sigma\{\angle\text{CPC}\} = 308.2(4)^\circ$ in Ph_3P as determined from averaging multiple crystal structures.²⁵ Advantages of this index over alternative descriptions of pyramidity include easy accommodation of deviations from full 3-fold symmetry and no need to define a principal axis.⁵² Systematic 2,6-disubstitution induces reduced pyramidity in PAr_3 , so that $\Sigma\{\angle\text{CPC}\} = 335.6(3)^\circ$ in Dipp_3P ,²⁶ $334.4(3)^\circ$ in Tripp_3P ,²⁸ and $329.1(5)^\circ$ in Mes_3P ,²⁹ all data taken from single-crystal diffraction studies. Pyramidity is also reduced upon oxidation, for example $\Sigma\{\angle\text{CPC}\}$ increases to $319.26(3)$ in Ph_3PO ,⁵³ to $317.5(4)^\circ$ in Ph_3PS ⁵⁴ and $317.9(6)^\circ$ in Ph_3PSe .⁵⁵ The pyramidity index of **1** is $303.5(2)^\circ$ for the P200,300,400 helical geometries, but $308.5(1)^\circ$ for the planar geometry of the P1 molecule in the measured crystal lattice. We can also compare $\Sigma\{\angle\text{CPC}\} = 313.31(5)^\circ$ in **5**, $314.69(5)^\circ$ in **6** and $315.28(10)^\circ$ in **7**. Interestingly, except for the planar geometry in **1**, all the *tris*(3,5-di-*tert*-butylphenyl)phosphine derivatives are consistently more pyramidal than simple $\text{Ph}_3\text{P(E)}$ analogues. Thus, we can now answer the question posed in the Introduction unequivocally: *endo* 5-*t*Bu groups do not generate steric pressure. In fact, they show an attractive rather than a repulsive interaction in the *endo* region.

The most likely origins for this attraction, resulting in increased pyramidity in **1 – 3** and **5 – 7**, are dispersion forces operating between the 3,5-substituent groups and the π electron density of these electron-rich aromatic rings. In support of this notion, the DFT calculations originally used in the data analysis were repeated at the same level of theory but incorporating Grimme's D3 empirical dispersion correction with geometry re-optimization for **1 – 4**.⁵⁶⁻⁶⁰ The results have decreased values of $\Sigma\{\angle\text{CPC}\}$ that correlate directly with the identity of the 3,5-substituents (Table 1).²² That is, $\Sigma\{\angle\text{CPC}\} > 305^\circ$ for 3,5- H_2 , $\Sigma\{\angle\text{CPC}\} = 304.8^\circ$ for 3,5-diMe (a small change) and 298.3° for 3,5-di^{*t*}Bu (a considerably larger contraction). The role of dispersion interactions with and between 3,5-dimethylphenyl groups has recently been recognized as supplying more energy towards holding the sterically challenged all-*meta* *tert*-butyl hexaphenylethane together than the C–C covalent bond [59].

Conclusions

Taken together, the structural properties for **1** and **5 – 7** demonstrate in their crystallography the challenges posed by 3,5-*bis-t*Bu group substitution. Parent phosphine **1** crystallizes as a complex cluster of four molecules with several different conformations. Oxide **5** has a surprisingly strong affinity for water but has trouble maintaining the common doubly-bridged $\text{P}=\text{O}\{\text{OH}_2\}_2\text{O}=\text{P}$ motif and has the longest ever reported separation between monomers among 30 such structures, which we attribute to distal steric congestion. Moreover, the structure suffers from multiple and different types of positional disorders. The structures of **6** and **7** have voids that are not filled by solvent but indicate that the bulky shapes have difficulty filling space efficiently.

Since greater pyramidity is associated with increased *s*-orbital contribution to the HOMO, the increasing pyramidity resulting from greater London dispersion forces also provides a plausible explanation for why the basicity of **1 – 3** are lower than expected based on isolated-ring indicators such as Hammett σ^+ constants or from the $^1J_{\text{P,Se}}$ coupling constants, from which changes in geometry must be excluded.⁴⁹ In view of the excellent correlation to DFT-calculated HOMO energies, we suggest that the phosphine donor strength of **1 – 4** established by voltammetry from anodic peak potentials are more accurate for this series than values obtained from $^1J_{\text{P,Se}}$. The interesting possibility that the conformational profiles of **1** and PPH_3 may be significantly affected by dispersion interactions, suggested by a referee, will be further investigated and reported on at a later time.

Experimental Section

General Methods. Solvents were reagent grade or better. THF (BDH) was dried by refluxing with Na/benzophenone. *Tris*(4-methoxyphenyl)phosphine, *tris*(4-methoxy-3,5-*bis*-dimethyl-phenyl)phosphine and *tris*(3,5-*bis*-dimethyl-phenyl)phosphine (Aldrich) were used as received as was 1-bromo-3,5-*tert*-butylbenzene (Aldrich). All work with air-sensitive phosphines was conducted in a dry N₂ atmosphere using modified Schlenk and vacuum line techniques. Elemental analyses for C, H, N, S were performed with a Vario Micro-cube Elemental Analyzer. FT-IR spectra were recorded on a Bruker Tensor 37 Spectrometer in the range of 4000–400 cm⁻¹. UV-Vis spectra (0.10 mmol solutions) were recorded on a Varian Cary 50 spectrophotometer using a quartz cell, in the range of 200–900 nm in CH₂Cl₂. NMR spectra were recorded in CDCl₃ solution (¹H, ¹³C and ³¹P) on a 300 MHz Bruker Avance II spectrometer and are referenced to the solvent residuals. The assignment of all the C and H resonances were confirmed by the 2D NMR techniques COSY, HSQC and HMBC. Archival NMR data is provided in Figures S6 – S9 in the SI.

Voltammetry. Cyclic voltammetry measurements were carried out at room temperature with a μ-Autolab (Type III, Metrohm-Eco Chemie) potentiostat/galvanostat. These experiments were performed using CH₃CN containing 0.10 M Bu₄NClO₄ (PTBA) as a supporting electrolyte and an electrochemical cell based on three electrodes: a 3 mm² glassy carbon working electrode, a platinum auxiliary electrode and an Ag/AgCl reference electrode in a Luggin capillary probe. Under these conditions, ferrocene (Fc) is oxidized at +0.375 V and the data are corrected to the Fc⁺⁰ scale. Voltammograms were performed over multiple scan rates ranging from 0.1 – 2.0 V·s⁻¹. A full set of CV scans and their scan-rate dependency is provided in Figures S10 and S11 in the SI.

Synthesis. *Tris*-(3,5-*di-tert*-butylphenyl)phosphine, **1** [189756-42-1].⁴ A solution of 5.0 g (18.6 mmol) of 1-bromo-3,5-*di-tert*-butylbenzene in 18 mL of dry THF in a 250 mL flask equipped with a side-arm stopcock was cooled to -78 °C for 10 min with stirring. Then 13.2 mL (19.5 mmol) of *n*BuLi (1.6 M in hexane) was added during 10 min. Thereafter, 0.540 mL (6.2 mmol) of PCl₃ was added over a further 10 min. The resulting mixture was warmed to 0°C and then stirred for 30 min. After removing all volatiles to a vacuum trap, the residue was quenched with a solution of 10 mL of H₂O and mL 1M cH₂SO₄ which had previously been degassed by boiling under N₂, followed by 2 x 20 mL of CH₂Cl₂ which had been deoxygenated by sparging with N₂. The organic phase (CH₂Cl₂ + phosphine) was transferred by canula to a clean flask containing anhydrous Na₂SO₄, the dried solution underwent a second canula transfer and was evaporated to leave 3.13 g of a white powder (yield: 84.4%). ¹H NMR (300.13 MHz, CDCl₃): δ H2 1.21 (s, 54H, -C(CH₃)₃); H1 7.06 (d, 6H, J_{H-P} = 9.0 Hz); H3 7.34 (s, 3H, -CH) (lit. δ: 1.22, 7.08, 7.36), in good agreement with the literature values.⁴ {¹H}-¹³C NMR (100.61 MHz, CDCl₃): 31.63 (s, ^tBu_{Me}), 35.14 (s, ^tBu_C), 122.42 (s, C_{para}), 128.18 (d, ²J_{CP} = 19 Hz, C_{ortho}), 137.25 (d, ¹J_{CP} = 9 Hz, C_{ipso}), δ 150.58 (d, ³J_{CP} = 6.4 Hz, C_{meta}) (lit. δ: 31.36, 34.83, 122.19, 127.94).⁴ {¹H}-³¹P NMR (121.49 MHz, CDCl₃): δ -1.30. IR (Diamond ATR, ν, cm⁻¹): 2951 s, 2897 m, 2867 m, 1578 m, 1472 m, 1418 m, 1388 m, 1365 s, 1286 w, 1239 s, 1197 w, 1124 m, 1016 w, 932 w, 901 m, 872 s, 781 w, 712 us, 583 m, 523 w, 475 m, 421 m (lit.: KBr 2950, 1575, 1475 cm⁻¹).⁴ For information on purification by recrystallization, see the SI.

Tris-(3,5-*di-tert*-butylphenyl)phosphine oxide monohydrate **5**. Leftovers of *tris*-(3,5-*di-tert*-butylphenyl)phosphine from various recrystallization attempts were placed in a 50 mL RB flask and dissolved in 20 mL of acetone. Thin-layer chromatography (elution: 95% hexanes; 5% ethyl acetate) was taken before reaction. Then the solution was heating with stirring to reflux and 4% aqueous H₂O₂ (0.7 mL of 30% H₂O₂ diluted with 5mL of H₂O) was added dropwise. Further TLC monitoring indicated reaction completion after 1 H. Crystals formed on cooling to RT and were filtered, taken up in 10 mL of CH₂Cl₂ and dried over anhydrous Na₂SO₄. After filtering and evaporation, the residue was recrystallized from 2 mL of boiling *n*-heptane. Cooling to -30°C afforded colourless crystals of a *hydrate* C₄₂H₆₃PO·*n*H₂O. 0.279 g. MP: 180–189 °C. Calc. for C₄₂H₆₃PO·0.35H₂O (best fit to residual water content; see Crystallography): C, 81.20; H, 10.34%. Found: C, 80.88; H, 9.96%. ¹H NMR (300.13 MHz, CDCl₃): δ H1 1.26 (s, 54H, -C(CH₃)₃); H1 7.46 (dd, 6H, J_{H-P} = 10.8 Hz);

H3 7.55 (t, 3H, -CH, $J_{H-H} = 1.8$ Hz) (lit. δ : 1.26, 7.48, 7.59).⁶ $\{^1\text{H}\}$ - ^{13}C NMR (75.48 MHz, CDCl_3): δ C_e 31.33 (s, -(CH₃)₃); C_d 35.01 (s, -C(CH₃)₃), C_f 125.55 (d, $^4J_{C-P} = 7$ Hz); C_b 126.45 (d, $^2J_{C-P} = 11$ Hz); C_a 132.18 (d, $^1J_{C-P} = 103$ Hz); C_c 150.61 (d, $^3J_{C-C} = 12$ Hz) (lit. δ : 31.3, 35.0, 126.2, 126.6, 130.2, 150.9).⁶ ^{31}P NMR (121.49 MHz, CDCl_3): δ +35.00. UV (dichloromethane, 5×10^{-5} mol·L⁻¹): $\lambda_{\text{max}} = 272$ nm ($\epsilon = 3128$), $\lambda_{\text{max}} = 280$ nm ($\epsilon = 2938$). IR (Diamond ATR, ν , cm⁻¹): 2954 s, 2903 w, 2857 w, 1587 w, 1479 m, 1425 m, 1388 w, 1359 m, 1239 m, 1184 m, 1148 s, 1016 w, 925 w, 896 w, 884 w, 871 m, 789 s, 711 s, 608 w, 529 s, 485 w, 448 s, 387 w.

Tris-(3,5-di-*tert*-butylphenyl)phosphine sulfide **6**. A 25 mL RB flask was charged with 300 mg (0.50 mmol) of **1** and 50 mg (0.19 mmol) of S₈ in 5 mL of *m*-xylene. The solution was refluxed with stirring for 2 H with periodic monitoring by TLC (hexanes). When all **1** was consumed, the cooled solution was evaporated to dryness. The residue was recrystallized from 6 mL of *n*-heptane at the boil, affording white crystals on cooling to RT which were filtered and dried (0.172 g, 57.3% yield). MP 240-250 °C. Calc. for C₄₂H₆₃PS: C, 79.94; H, 10.06; S, 5.08 %. Found: C, 80.18; H, 9.79; S, 4.90 %. ^1H NMR (300.13 MHz, CDCl_3): δ H2 1.24 (s, 54H, -C(CH₃)₃); H1 7.46 (dd, 6H, $J_{H-P} = 14.40$ Hz); H3 7.50 (t, 3H, -CH, $J_{H-H} = 1.8$ Hz). ^{13}C NMR (75.48 MHz, CDCl_3): δ C_e 31.29 (s, -(CH₃)₃); C_d 35.06 (s, -C(CH₃)₃), C_f 125.21 (d, $^4J_{C-P} = 3$ Hz); C_b 127.57 (d, $^2J_{C-P} = 11$ Hz); C_a 131.50 (d, $^1J_{C-P} = 76$ Hz); C_c 150.70 (d, $^3J_{P-C} = 12$ Hz). ^{31}P NMR (121.49 MHz, CDCl_3): δ +47.92. UV-vis (dichloromethane, 5×10^{-5} mol·L⁻¹): $\lambda_1 = 282$ nm ($\epsilon = 8216$), $\lambda_2 = 274$ nm ($\epsilon = 10158$). IR (Diamond ATR, ν , cm⁻¹): 2955 m, 2897 w, 2868 w, 1591 w, 1474 m, 1422 m, 1393 m, 1358 m, 1247 m, 1195 w, 1139 m, 1129 s, 1021 w, 922 w, 896 w, 882 w, 857 w, 780 m, 707 s, 661 w, 588 m, 527 m, 480 w, 437 m.

Tris-(3,5-di-*tert*-butylphenyl)phosphine selenide **7**. A 25 mL RB flask was charged with 300 mg (0.50 mmol) of **1** and 210 mg (2.66 mmol) of gray Se in 5 mL of *m*-xylene. The solution was refluxed with stirring for 2 H with periodic monitoring by TLC (95% hexanes/5% ethyl acetate). The solution was then cooled to RT and filtered through a plug of Celite™ to remove excess Se. The residue was evaporated and then recrystallized from 6 mL of *n*-heptane which on cooling to RT afforded white crystals (0.1 g, 37% yield). MP 274-278 °C. Calc. for C₄₂H₆₃PSe: C, 74.42; H, 9.37%. Found: C, 73.96; H, 8.91%. ^1H NMR (300.13 MHz, CDCl_3): δ H2 1.4 (s, 54H, -C(CH₃)₃); H1 7.44 (dd 6H, $J_{H-P} = 14$ Hz); H3 7.50 (t, 3H, -CH, $J_{H-H} = 1.5$ Hz). ^{13}C NMR (75.48 MHz, CDCl_3): δ C_e 31.29 (s, -(CH₃)₃); C_d 35.06 (s, -C(CH₃)₃), C_f 125.21 (d, $^4J_{C-P} = 3$ Hz); C_b 126.95 (d, $^2J_{C-P} = 11$ Hz); C_a 131.5 (d, $^1J_{C-P} = 76$ Hz); C_c 150.70 (d, $^3J_{P-C} = 12$ Hz). ^{31}P NMR (121.49 MHz, CDCl_3): δ +39.54 ($J_{P-Se} = 719$ Hz). Lit value δ +37.4 ($J_{P-Se} = 714.0$ Hz).³ UV-vis (dichloromethane, 5×10^{-5} mol·L⁻¹): $\lambda_1 = 273$ nm ($\epsilon = 8960$), $\lambda_2 = 441$ nm ($\epsilon = 566$), $\lambda_3 = 505$ nm ($\epsilon = 398$), $\lambda_4 = 692$ nm ($\epsilon = 226$). IR (Diamond ATR, ν , cm⁻¹): 2955 s, 2902 w, 2862 w, 1586 w, 1468 m, 1416 m, 1393 w, 1358 s, 1247 s, 1195 w, 1130 s, 1019 w, 926 w, 898 w, 878 w, 859 w, 787 m, 774 w, 706 w, 607 w, 587 m, 528 s, 499 s, 479 w, 436 s, 389 w.

Crystallography. The structures of **1** and **5** – **7** were determined by single crystal X-ray crystallography at 100 K on a Rigaku-Oxford Diffraction SuperNova diffractometer equipped with a Pilatus P200 HPAD detector and using Cu K_{α} radiation, $\lambda = 1.54184$ Å. Crystals were coated in Paratone™ oil, mounted on a MiTeGen loop and cooled to 100(1) K on the goniometer using the cold gas from an Oxford Cryostream 800. The images were integrated, the data processed and corrected for absorption using CrysAlisPro 1.171.38.43, solved with SHELXT,⁶¹ and refined using SHELXL-2014⁶² within the Olex2 suite of programs.⁶³ Only the structure of **6** was fairly straightforward with only some ^tBu rotational disorder to account for. Full details regarding the solution and refinement of these structures, including superlattice effects, are provided in the SI, along with tables of crystal and data collection parameters (Tables S1) and derived parameters (Table S2). Graphical output of the full structure of **1** is provided in Figure S1. Comparisons of the ‘flat’ and helical conformations in **1** with structures found in metal complexes and by computation are in Figure S2. A supercell refinement of **5** is depicted in Figure S3 and various space-filling shapes in Figures S4 and S5. Structures were visualized and

analyzed using Mercury CSD.⁶⁴ The crystallographic data have been deposited at the Cambridge Crystallographic Data Centre as CCDC 1834017 – 1834020.

Acknowledgements

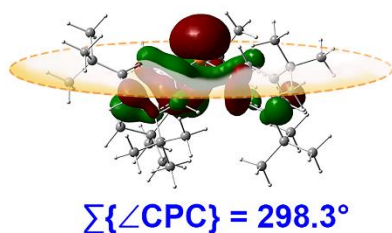
The authors thank the Brazilian agencies (CNPq PVE 401271/2014-5 and CAPES) and the NSERC-Canada (Discovery Grant to RTB) for generous financial support. We especially acknowledge the University of Lethbridge for purchasing the SuperNova X-ray diffractometer. We thank Dr. Eric Reinheimer of Rikagu Americas for providing significant assistance with the disorder models and data processing for some of the crystal structures.

- [1] M. Naruto, S. Saito, *Nat. Commun.* **2015**, 6:8140 (doi: 10.1038/ncomms9140).
- [2] B. Vulovic, A. P. Cinderella, D. A. Watson, *ACS Catal.* **2017**, 7, 8113-8117.
- [3] A. P. Cinderella, B. Vulovic, D. A. Watson, *J. Am. Chem. Soc.* **2017**, 139, 7741-7744.
- [4] K. Manabe, *Tetrahedron*, **1998**, 54, 14465-14476. The authors of ref. [3] have ascribed a name to **1**, "DREWphos". Whatever the merits are of trying to name compounds after lab employees, it seems unethical to ignore the right of discovery. We respectfully suggest it should be called MANABEphos.
- [5] M. Ullrich, A. J. Lough, D. W. Stephan, *Organometallics* **2010**, 29, 3647-3654.
- [6] M. Szigeti, Z. Dobi, T. Soós, *J. Org. Chem.* **2018**, 83, 2869-2874.
- [7] D. Gust, K. Mislow, *J. Am. Chem. Soc.* **1972**, 95, 1535-1547.
- [8] J. D. Andose, K. Mislow, *J. Am. Chem. Soc.* **1974**, 96, 2128-2167.
- [9] K. Mislow, *Acc. Chem. Res.* **1976**, 9, 26-33.
- [10] M. R. Kates, J. D. Andose, P. Finocchiaro, D. Gust, K. Mislow, *J. Am. Chem. Soc.* **1977**, 99, 1772-1778.
- [11] M. Landman, T. Levell, P. H. van Rooyen, J. Conradie, *J. Mol. Struct.* **2014**, 1065-1066, 29-38.
- [12] S. Rizzo, R. Cirilli, M. Pierini, *Chirality* **2014**, 26, 601-606.
- [13] B. Laleu, G. Bernardinelli, R. Chauvin, J. Lacour, *J. Org. Chem.* **2006**, 71, 7412-7416.
- [14] S. Sasaki, M. Yoshifuji, *Curr. Org. Chem.* **2007**, 11, 17-31.
- [15] T. Benincori, V. Bonometti, R. Cirilli, P. R. Mussini, A. Marchesi, M. Pierini, T. Pilati, S. Rizzo, F. Sannicolò, *Chem. Eur. J.* **2013**, 19, 165-181.
- [16] C. Puigjaner, S. Vela, M. Font-Bardiac, J. J. Novoa, *CrystEngComm* **2014**, 16, 8214-8223.
- [17] L. Dubován, A. Pöllnitz, C. Silvestru, *Eur. J. Inorg. Chem.* **2016**, 1521-1527.
- [18] J. F. Costello, S. G. Davies, E. T. F. Gould, J. E. Thomson, *Dalton Trans.* **2015**, 44, 5451-5466.
- [19] J. Conradie, *Dalton Trans.* **2012**, 41, 10633-10642.
- [20] J. F. Costello, S. G. Davies, *J.C.S. Perkins Trans.* **1998**, 2, 1683-1689.
- [21] H. Brunner, R. Oeschey, B. Nuber, *Angew. Chem. Int. Ed. Engl.* **1994**, 33, 866-868.
- [22] N. D. D. Hill, R. T. Boéré, *Acta Crystallogr., Sect. E: Crystallogr. Commun.* **2018**, E74, 889-894.
- [23] U. Hengartner, D. Valentine, Jr., K. K. Johnson, M. E. Larscheid, F. Pigott, F. Scheidl, J. W. Scott, R. C. Sun, J. M. Townsend, T. H. Williams, *J. Org. Chem.* **1979**, 44, 3741-3747.
- [24] J. K. Romain, J. W. Ribblett, R. W. Byrn, R. D. Snyder, B. N. Storhoff, J. C. Huffman, *Organometallics* **2000**, 19, 2047-2050.
- [25] J. Bruckmann, C. Krüger, F. Lutz, *Z. Naturforsch.* **1995**, 50b, 351-360.
- [26] R. T. Boéré, A. M. Bond, S. Cronin, N. W. Duffy, P. Hazendonk, J. D. Masuda, K. Pollard, Kyle; T. L. Roemmele, P. Tran, Y. Zhang, *New J. Chem.* **2008**, 32, 214-231.
- [27] J. P. Bullock, A. M. Bond, R. T. Boéré, T. M. Gietz, T. L. Roemmele, S. D. Seagrave, J. D. Masuda, M. Parvez, *J. Am. Chem. Soc.* **2013**, 135, 11205-11215.
- [28] S. Sasaki, K. Sutoh, F. Murakami, M. Yoshifuji, *J. Am. Chem. Soc.* **2003**, 124, 14830-14831.
- [29] J. F. Blount, D. Camp, R. D. Hart, P. C. Healy, B. W. Skelton, A. H. White, *Aust. J. Chem.* **1994**, 47, 1631-1639.

- [30] M. Alcarazo, *Acc. Chem. Res.* **2016**, *49*, 1797-1805.
- [31] E. Haldón, Á. Kozma, H. Tinnermann, L. Gu, R. Goddard, M. Alcarazo, *Dalton Trans.* **2016**, *45*, 1872-1876.
- [32] H. Tinnermann, C. Wille, M. Alcarazo, *Angew. Chem. Int. Ed.* **2014**, *53*, 8732–8736.
- [33] R. T. Boéré, Y. Zhang, *J. Organomet. Chem.* **2005**, *690*, 2651-2657.
- [34] T. Iwai, M. Sawamura, *Bull. Chem. Soc. Jpn.* **2014**, *87*, 1147–1160.
- [35] H. Ohta, M. Tokunaga, Y. Obora, T. Iwai, *Org. Lett.* **2007**, *9*, 89-92.
- [36] Y. Ohzu, K. Goto, H. Sato, T. Kawashima, *J. Organomet. Chem.* **2005**, *690*, 4175-4183.
- [37] Y. Ohzu, K. Goto, T. Kawashima, *Angew. Chem. Int. Ed. Engl.* **2003**, *42*, 5714-5717.
- [38] K. M. Steed, J. W. Steed, *Chem. Rev.* **2015**, *115*, 2895-2933.
- [39] C. P. Brock, *Acta Crystallogr., Sect. B: Struct. Sci.* **2016**, *72*, 807–821.
- [40] F. H. Allen, *Acta Crystallogr., Sect. B: Struct. Sci.* **2002**, *58*, 380–388.
- [41] R. S. Cahn, C. Ingold, V. Prelog, *Angew. Chem., Int. Ed. Engl.* **1966**, *5*, 385-415.
- [42] Centrosymmetry over the whole unit cell ensures that there are six of each *M* and *P* enantiomer in the racemic crystal.
- [43] The Durham University *Z'* database is now located at <http://zprime.co.uk/>.
- [44] P. G. Jessop, M. M. Olmstead, C. D. Ablan, M. Grabenauer, D. Sheppard, C. A. Eckert, C. L. Liotta, *Inorg. Chem.* **2002**, *41*, 3463-3468.
- [45] O. bin Shawkataly, M. A. A. Pankhi, M. I. Mohamed-Ibrahim, M. R. Hamdan, H.-K. Fun, *Acta Crystallogr., Sect. E: Struct. Rep. Online* **2009**, *65*, o1080.
- [46] J. A. S. Howell, N. Fey, J. D. Lovatt, P. C. Yates, P. McArdle, D. Cunningham, E. Sadeh, H. E. Gottlieb, Z. Goldschmidt, M. B. Hursthouse, M. E. Light, *J. Chem. Soc., Dalton Trans.* **1999**, 3015-3028.
- [47] M. Culcasi, Y. Berchadsky, G. Gronchi, P. Tordo, *J. Org. Chem.* **1991**, *56*, 3537-3542.
- [48] J. E. Leffler, E. Grunwald, *Rates and Equilibria of Organic Reactions*, Wiley, 1963 (Dover reprint).
- [49] U. Beckmann, D. Süslüyan, P. Kunz, *Phos. Sulf. Sil. Rel. Elem.* **2011**, *186*, 2061–2070.
- [50] R. T. Boéré, Y. Zhang, *Acta Cryst., Sect. C: Cryst. Struct. Comm.* **2013**, *69*, 1051-1054.
- [51] D. J. Brauer, M. Hingst, K. W. Kottsieper, C. Like, T. Nickel, M. Tepper, O. Stelzer, W. S. Sheldrick, *J. Organomet. Chem.* **2002**, *645*, 14-26.
- [52] An earlier definition of the "fold back" angle α was a useful tool to describe pyramidality in the era of using Z-matrices to describe geometries – see ref. 47. An average value for α can be defined from our pyramidality index: $\alpha = \cos^{-1}[\{\sin(\angle\text{CPC}/6)/\cos 30^\circ\}]$.
- [53] J. A. Thomas, T. A. Hamor, *Acta Crystallogr., Sect. C: Cryst. Struct. Commun.* **1993**, *49*, 355-357.
- [54] T. Schulz, K. Meindl, D. Leusser, D. Stern, J. Graf, C. Michaelsen, M. Ruf, G. M. Sheldrick, D. Stalke, *J. Appl. Crystallogr.* **2009**, *42*, 885-891.
- [55] P. W. Coddling, K. A. Kerr, *Acta Crystallogr., Sect. B: Struct. Crystallogr. Cryst. Chem.* **1979**, *35*, 1261-1263.
- [56] S. Grimme, J. Antony, S. Ehrlich, H. Krieg, *J. Chem. Phys.* **2010**, *132*, 154104.
- [57] C. Bannwarth, S. Grimme, *J. Chem. Phys.*, **2017**, *147*, 034112.
- [58] G. Bistoni, A. A. Auer, F. Neese, *Chem. Eur. J.*, **2017**, *23*, 865-873.
- [59] S. Rösel, C. Balestrieri, P. R. Schreiner, *Chem. Sci.*, **2017**, *8*, 405-410.
- [60] C. Esterhuysen, A. Heßelmann, T. Clark, *Chem. Phys. Chem.*, **2017**, *18*, 772-784.
- [61] G. M. Sheldrick, *Acta Crystallogr., Sect. A: Foundat. Adv.* **2015**, *71*, 3-8.
- [62] G. M. Sheldrick, *Acta Crystallogr., Sect. C: Struct. Chem.* **2015**, *71*, 3-8.
- [63] O. V. Dolomanov, L. J. Bourhis, R. J. Gildea, J. A. K. Howard, H. Puschmann, *J. Appl. Cryst.* **2009**, *42*, 339-341.

- [64] C. F. Macrae, I. J. Bruno, J. A. Chisholm, P. R. Edgington, P. McCabe, E. Pidcock, L. Rodriguez-Monge, R. Taylor, J. van de Streek, P. A. Wood, *J. Appl. Cryst.* **2008**, *41*, 466-470.

Graphical Abstract and TOC Text



MANABEphos, valued as a supporting ligand because of the distal steric bulk from the *exo*-oriented *tert*butyl groups, is also rendered more pyramidal than PPh₃ through London dispersion forces on and between the *endo*-substituents, which results in a raised HOMO energy and reduced basicity